Journal of Environmental Chemical Engineering 11 (2023) 109947

Contents lists available at ScienceDirect

Journal of Environmental Chemical Engineering

journal homepage: www.elsevier.com/locate/jece

Strong Metal-Support Interaction (SMSI) in Au/TiO_2 photocatalysts for environmental remediation applications: Effectiveness enhancement and side effects

Manuel Luna [a], Adrian Gonzalez-Hidalgo [a,b], Ana Diaz [a], Daniel Goma [b], José Manuel Gatica [b,*], María Jesús Mosquera [a]

[a] TEP-243 Nanomaterials Group, Departamento de Química Física, Facultad de Ciencias, Universidad de Cádiz, Puerto Real 11510, Spain
[b] Departamento de Ciencia de los Materiales e Ingeniería Metalúrgica y Química Inorgánica e IMEYMAT, Universidad de Cádiz, Puerto Real 11510, Spain

ARTICLE INFO

Editor: Stefanos Giannakis

Keywords:
Au/TiO_2
SMSI
Soot
Environmental Photocatalysis
NO_x

ABSTRACT

Strong Metal−Support Interaction (SMSI) is a well-known phenomenon of heterogeneous catalysis that have not been extensively investigated in photocatalytic applications. Moreover, the reactions previously studied for photocatalysts under SMSI state are mainly restricted to energy related uses. The present work seeks to explore the effect of SMSI induced by soft wet-chemistry in a Au/TiO_2 photocatalyst with specific focus on photocatalytic environmental remediation. With this aim, the developed photocatalyst has been evaluated considering liquid, gas and solid pollutants in order to represent the wide range of environmental photocatalysis applications. These photooxidation scenarios were methylene blue dissolved in water, gaseous NO, and soot directly deposited on the photocatalyst. The results revealed that the SMSI induction has a generally positive effect on photoactivity promoting the MB and soot removal by 53% and 60%, respectively. However, the SMSI did not provide any additional benefit in the NO_x elimination compared to the non-SMSI Au/TiO_2 photocatalyst, because the enveloping of AuNPs limits the gold-pollutant interaction.

1. Introduction

The Metal-Support Interaction (MSI) strongly affects activity of metal supported catalysts [1]. Similarly, this interaction also modifies the photocatalytic properties of semiconductors when a metal is deposited on them [2]. Since noble metals, such as gold and platinum, are the most appropriate for the photoactivity enhancement, the maximization of the MSI is an effective way to optimize the employment of these expensive elements. The Au/TiO_2 photocatalysts would probably be the most studied metal-TiO_2 photocatalytic system and the literature is riddled with all sorts of works where different characteristics of these photocatalysts are modified [3]. The change of gold dispersion is one of the most direct ways of modifying the Au-TiO_2 interaction, since the gold nanoparticles (AuNPs) size affects the Schotky barrier produced by the TiO_2-Au contact and the resultant Fermi level [4], as well as the electronic transference processes from Au to TiO_2 after gold plasmon excitation [5]. Other strategies for modifying the Au-TiO_2 interaction are based on the geometrical control of AuNPs [6] and TiO_2 support [7].

The Strong Metal–Support Interaction (SMSI) is a particular type of MSI that is well-known in heterogeneous catalysis. The SMSI was discovered by Tauster et al. for platinum group metal supported on TiO_2 catalysts in the late 1970 s [8], while noting that these catalysts lost its CO and H_2 adsorption capacities after a high temperature reduction treatment. It had initially been proposed that this phenomenon was a consequence of the formation of bonds or intermetallic compounds between the noble metal and titanium, but it was later demonstrated that SMSI is generated because the metal is covered or totally encapsulated by the support [9,10]. The SMSI induction has been widely studied in heterogeneous catalysis as a method to increase the stability and/or to promote the activity of metal supported catalysts, mainly in reactions like the CO_2 hydrogenation or those dealing with the generation/purification of H_2 [11]. Despite the SMSI was restricted to platinum group metal catalysts during years, it was recently realised for gold catalysts supported on ZnO [12] and TiO_2 [13].

Even though the photocatalysts with embedded metal nanoparticles, such as the core-shell structures [14], have been frequently exploited to increase the MSI and promote the photocatalytic activity, the research about SMSI in photocatalytic applications has been much less

* Corresponding author.
E-mail address: josemanuel.gatica@uca.es (J.M. Gatica).

https://doi.org/10.1016/j.jece.2023.109947
Received 27 February 2023; Received in revised form 10 April 2023; Accepted 15 April 2023
Available online 17 April 2023

significant. Specifically, most of these studies deal with Pd/TiO_2 and Pt/TiO_2 photocatalysts [15–17], being the literature about gold group metals very scarce [18]. Despite the lack of results, the previous findings suggest that SMSI has a positive effect on photoactivity, being a possible method for optimizing Au/TiO_2 photocatalysts and enhancing the performance of different photocatalytic processes. In addition to the classical methods for SMSI induction based on thermal treatments at high temperature under reducing atmosphere, wet chemistry methods for obtaining the SMSI under mild conditions have been developed [19]. This last methodology is of special interest because the high temperatures conventionally employed can produce gold sintering but also alterations on TiO_2 support modifying the crystalline phases, surface area and the resultant activity [20]. Despite some Au/TiO_2 photocatalysts can resist relatively high temperatures, the photocatalysts composed by nanoparticles with non-thermodynamically stable geometries are more susceptible to the heating [21,22], being mandatory the soft methods for reaching the SMSI state in order to minimize the temperature side effects.

With this aim, the present work investigates how the SMSI effect can affect the photoactivity of low gold loadings and high metal dispersions Au/TiO_2, with a special emphasis on environmental applications. In view of the lack of information concerning the performance of Au/TiO_2 photocatalyst in SMSI state, a proper characterization and wide evaluation has been performed. Specifically, three types of photocatalytic reactions have been chosen in order to study the photocatalytic performance simulating three different photooxidation scenarios: 1) molecules dissolved in water (methylene blue in water), 2) gas molecules (NO) and 3) solid substance directly deposited on the photocatalyst (soot). These reactions can also be considered representative examples of real photocatalytic applications, such as the elimination of pollutants in water and air, and the self-cleaning surfaces.

2. Experimental

2.1. Photocatalysts synthesis

A Au/TiO_2 photocatalyst was prepared with a 1.24% wt% nominal gold loading employing the classical deposition-precipitation method of Haruta [23]. $KAuCl_4$ (99.995% purity from Sigma-Aldrich) was dissolved in 300 ml of distilled water, the pH of solution was adjusted to 8 using 1 M NaOH solution, 3 g of TiO_2 Aeroxide P25 from Evonik (according to the manufacturer: BET SSA 50 ± 15 m^2/g, anatase/rutile ratio 80/20 and primary particle size 21 nm) was added and the pH was readjusted to 8. The suspension was heated at 80 °C under vigorous stirring for 2 h. The obtained slurry was centrifuged and redispersed in water three times in order to remove any synthesis residues, being negative the chloride test using $AgNO_3$. The obtained solid was dried at 100 °C overnight, ground using an agate mortar and calcined at 300 °C for 4 h.

The strong metal support interaction (SMSI) was induced in the Au/TiO_2 photocatalysts through a wet-chemistry method proposed by Zhang et al. [19]. Accordingly, 1 g of the previously prepared Au/TiO_2 sample was dispersed in 60 ml of H_2O. A TiO_x sol was prepared by dissolving 77 mg of $TiCl_3$ solution (12% in hydrochloric acid from Sigma-Aldrich) in 10 ml of H_2O and adding 18 mg of $NaHCO_3$. This sol was added dropwise to the photocatalyst suspension under vigorous stirring. After stirring for 1 h, 1 ml of 1 M $NaHCO_3$ aqueous solution was added dropwise and the mixture was stirred for another 2 h. The resultant solid was washed, dried and calcined following the same procedure described above, except that the calcination time was 1 h. This sample was designed as Au/TiO_2-SMSI.

2.2. Photocatalysts characterization

The gold content of photocatalysts was determined by Inductively Coupled Plasma Atomic Emission Spectroscopy (ICP-AES) using an Iris Intrepid spectrophotometer from Thermo Scientific.

The acid-base behaviour of the photocatalysts was studied measuring the pH of an aqueous dispersion of the photocatalysts. 20 mg of photocatalyst was dispersed in 10 ml of water in an ultrasound bath during 10 min. The previous dispersions were diluted 1:3 in order to study the zeta potential and hydrodynamic size by dynamic light scattering (DLS) using a Zetasizer Nano Z analyser from Malvern Instruments.

N_2 physisorption at − 196 °C was performed using an Autosorb iQ3 gas sorption analyser from Quantachrome. Approximately 0.125 g of samples, previously outgassed at 200 °C under vacuum, were employed. The Brunauer-Emmett-Teller specific surface area (BET SSA) was determined using the multipoint BET method within the P/P_0 interval 0.05–0.2 and the Barrett-Joyner-Halenda (BJH) pore size distributions were calculated from the isotherm desorption branches.

The UV–visible absorption spectra of the photocatalysts were obtained by diffuse reflectance spectroscopy using a UV-2600 spectrophotometer equipped with an ISR-2600 integrating sphere from Shimadzu. The photocatalysts band gap values were calculated by using the Kubelka-Munk function and the Tauc plot [24,25].

The X-Ray Photoelectron Spectroscopy (XPS) characterization of the samples was performed on an Axis Ultra DLD spectrometer from Kratos using Al K_α radiation (1486.6 eV) and operating at 150 W. The photocatalysts samples were previously pressed as pellets and the survey and relevant high resolution core levels spectra were recorded. The binding energy (BE) scale was corrected using the C 1 s core level from adventitious carbon at 284.8 eV.

The transmission electron microscopy characterization was carried out using a Talos F200X G2 microscope from Thermo Fisher Scientific operated at 200 kV in High-Resolution (HRTEM) and High-Angle Annular Dark-Field Scanning Transmission (HAADF−STEM) modes with resolutions of 0.12 and 0.16 nm, respectively.

CO chemisorption measurements were conducted using a Micromeritics ASAP 2020 C automatic analyser. The apparent equilibrium data for the obtained isotherms were considered to be reached when the pressure change was less than 5% for 11 consecutive readings taken at 8-s intervals. The analyses were carried out using approximately 0.25 g of sample at − 80 °C in order to minimize the possible contribution of spillover effects [26]. Two consecutive isotherms separated by an intermediate evacuation under vacuum (30 min) were carried out. The CO specifically adsorbed on Au can be determined subtracting the second isotherm of bare support from the second isotherm of the corresponding gold containing photocatalyst [27]. The amount of CO adsorbed specifically on AuNPs was calculated using the values of CO adsorbed at 200 torr. The TiO_2 P25 sample was previously calcined at 300 ºC (4 h) to make it comparable to the gold-loaded samples.

2.3. Photocatalysts performance evaluation

Methylene blue (MB) aqueous solution decolourization tests were employed to study the capacity of the photocatalysts for degrading organic molecules in aqueous media. A photocatalysts aqueous suspension (100 mg/200 ml) was sonicated in an ultrasound bath for 15 min and 2 ml of MB solution 1 mM was added in order to get a MB concentration nearly 10^{-5} M. The suspension was kept under vigorous stirring in dark conditions for 30 min to ensure the complete MB adsorption on TiO_2 before the light irradiation. Two light sources were employed: UV radiation from a 15 W fluorescent backlight bulb lamp and UV-Vis radiation from an Ultra Vitalux 300 W lamp from Osram. In both cases the lamp position was adjusted in order to obtain an irradiance of 1 mW/cm^2 in the range 300–400 nm. Sample aliquots were obtained at progressive irradiation times and their UV-Visible spectra were recorded using the UV-2600 spectrophotometer, after filtration through a 0.45 μm syringe filter. The degradation plots were represented using the Abs/Abs_0 at 664 nm and the results were fitted to a first order rate equation.

The depolluting properties of photocatalysts for removing air

pollutants were evaluated through NO photooxidation tests according to the ISO 22197–1 standard [28]. An aqueous dispersion containing 50 mg of photocatalysts and 50 mg of $Ca(OH)_2$ were deposited on 10×5x 0.4 cm glass plates, obtaining the photocatalytic layer after evaporation. The sample was placed in a PMMA reactor connected to the gas system, the NO in air (1000 ppb 50% relative humidity) flowed through the reactor and after stabilization of NO concentration the sample was irradiated with the Osram Ultra Vitalux lamp for two hours. The concentrations of NO, NO_x and NO_2 were measured by chemiluminescence using a model 42i analyser from Thermo Scientific.

The amount of NO converted, NO_2 generated and NO_x removed were calculated by integration of concentration profiles during the light irradiation periods as described in the standard procedure above mentioned and the results were expressed as percentages using the following equations:

$$\%\ \mathrm{NO\ conversion} = 100\frac{n_{NO}}{n_{NO\,total}}$$

$$\%\ NO_2\ \mathrm{generated} = 100\frac{n_{NO_2}}{n_{NO\,total}}$$

$$\%\ NO_x\ \mathrm{removed} = 100\frac{n_{NO} - n_{NO_2}}{n_{NO\,total}}$$

where n_{xx} are the μmol of the corresponding gas.

The selectivity of the process towards NO_2 formation of the process was calculated as follows:

$$\%\ NO_2\ \mathrm{selectivity} = 100\cdot\frac{n_{NO_2}}{n_{NO}}$$

The $DeNO_x$ index [29] was calculated using the next equation:

$$DeNO_x = \%\ \mathrm{NO\ conversion} - 3(\%\ NO_2\ \mathrm{generated})$$

Finally, soot was chosen to evaluate the photoelimination of solid polluting substances deposited on the photocatalyst. The samples were prepared depositing 20 mg of photocatalyst on 2.5 × 7.5 cm microscope glass slides following the same procedure employed for NO evaluation samples without $Ca(OH)_2$ addition. Non-photocatalytic samples were also prepared by deposition of SiO_2 Aerosil OX50 from Evonik (fumed silica with BET SSA 50 ± 15 m^2/g and average particle size of 40 nm). Soot was deposited exposing the sample to a hexane flame according to the following procedure. The sample was disposed face down over a porcelain crucible at a height of 12 cm and 1 ml of hexane was burnt in the crucible for producing the soot layer. This method produced a soot layer with an estimated thickness of 0.35 μm, according to the absorbance of the soot layer deposited in a non-coated glass slide and considering a soot absorption coefficient of 2×10^4 cm^{-1} at 350 nm [30]. The samples were irradiated with UV–vis light from the Osram Ultra Vitalux lamp at an irradiance of 2 mW/cm^2 in the range 300–400 nm. The UV-Vis spectra of the samples were recorded at different irradiation time employing the previously described spectrophotometer. The soot elimination was quantified considering the Abs/Abs_0 at 420 nm and the results were fitted to a first order rate equation.

For all the photodegradation studies the measurements were carried out by duplicate.

3. Results and discussion

3.1. Characterization

The compositional analysis of Au/TiO_2 photocatalysts revealed that the wet-chemical process for SMSI induction did not modify the gold loading of the starting material (Table 1). On the other hand, the gold deposition on TiO_2 produced an evident change in the acid-base behaviour of TiO_2 increasing their pH in water dispersion by two points, that remains similar in the Au/TiO_2-SMSI sample (Table 1). The water dispersibility of photocatalysts was also reduced significantly after the synthesis processes, which was demonstrated by the determination of photocatalyst hydrodynamic sizes by DLS technique (Fig. 1 and Table 1). The size distribution of TiO_2 was centred around 100 nm which corresponds to low size agglomerates composed by a small number of particles [31], contrarily to the Au/TiO_2 and Au/TiO_2-SMSI photocatalysts in which larger agglomerates in the micrometric range were produced. This agglomeration can be directly related to the change of acid-base behaviour of the photocatalysts. In this sense, both Au/TiO_2 and Au/TiO_2-SMSI samples exhibited pH values close to the isoelectric point of TiO_2 P25 that is around 6.5 [32]. In this situation, the TiO_2 charge will be low promoting the particle agglomeration due to the lack of electrostatic repulsion. The Z potential measurements (Table 1) confirmed this interpretation, showing the Au/TiO_2 sample a Z potential considerably lower than TiO_2 while Au/TiO_2-SMSI exhibited a value very close to 0. Additionally, the titanium oxide overlayer of Au/TiO_2-SMSI could act bonding the TiO_2 particles making their dispersion more difficult. The N_2 physisorption isotherms of the photocatalysts are showed in Fig. S1 as Supplementary Information. TiO_2 sample showed a type II isotherm which is related to the presence of macropores but with H3 hysteresis revealing also the existence of mesoporosity [33]. Both gold-containing photocatalysts exhibited similar type II isotherms with H1 hysteresis that is characteristic of mesoporous materials with a nanoparticle aggregate structure [34]. Despite these differences, there are not significant changes in the photocatalysts specific surface area (Table 1), indicating that TiO_2 sintering was not produced by neither the AuNPs deposition nor SMSI induction processes. On the contrary, the BJH pore size distributions substantially changed after the AuNPs deposition (Fig. S2 in Supplementary Information). TiO_2 exhibited a wide pore distribution centred around 60 nm, confirming the presence of macropores responsible for the H3 hysteresis. These pore

Table 1
Results of compositional and physicochemical characterization of the photocatalyts.

	TiO_2	Au/TiO_2	Au/TiO_2-SMSI
Au loading (wt%)[a]	-	0.99 ± 0.02	0.98 ± 0.02
pH	4.4	6.5	6.3
Hydrodynamic size (nm)[b]	124	1020	2261
Z potential (mV)[b]	14.7	3.5	-0.6
BET SSA (m^2/g)[c]	58	56	55
Average pore diameter (nm)[c]	62	34	35
CO chemisorbed (mmol/g)	-	0.020	0.009

[a] determined by ICP-AES; [b] obtained by DLS; [c] from N_2 physisorption

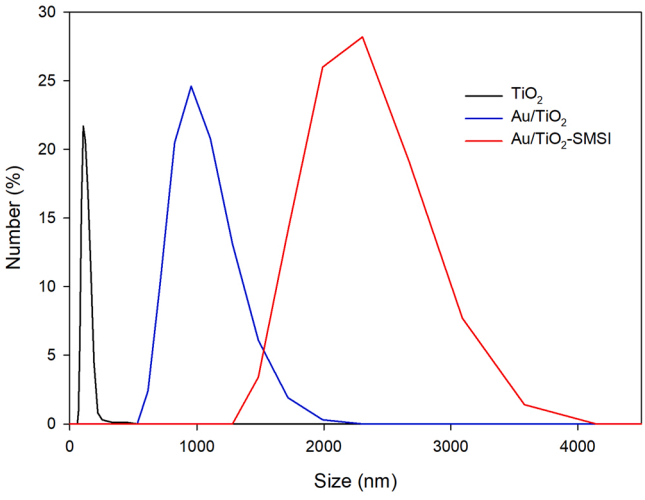

Fig. 1. DLS hydrodynamic size distributions.

sizes are considerably higher than the P25 average size (25 nm) indicating a very low particle compaction, which was in line with its low tapped density (0.12 g/cm^3) compared to the TiO_2 bulk density (4.23 g/cm^3). On the other hand, Au/TiO_2 and Au/TiO_2-SMSI showed nearly identical pore sizes distributions that were considerably narrower and centred at approximately 35 nm, size closer to P25 dimensions. This can be attributed to a higher compaction of TiO_2 particles that decrease the interparticle distance and, consequently, the pore size due to the wetting and drying processes that these photocatalysts underwent.

The intense purple colour of the photocatalysts containing AuNPs clearly indicated the presence of the gold localized surface plasmon resonance (LSPR) band as observed in the UV–vis absorption spectra (Fig. 2). The maximum of LSPR band was located at 558 nm for Au/TiO_2 photocatalyst, a significant redshift in comparison with AuNPs in aqueous media [35], which is related to the change of the media surrounding the AuNPs [36]. In the case of Au/TiO_2-SMSI, the band was slightly shifted to 563 nm and its width increased from 178 to 194 nm. This change in the LSPR band may be an evidence of the covering of AuNPs with a thin TiO_2 layer, because the high refractive index of TiO_2 has a strong influence on the plasmon [37]. The UV absorption associated to the band-to-band transition of TiO_2 was also modified by the presence of AuNPs resulting in a decrease of band gap values. The calculated band gap for bare TiO_2 was 3.24 eV, very close to the value for anatase (3.2), and decreased to 3.09 eV for Au/TiO_2. This band gap decrease can be related to the presence of new energetic levels associated with the Schottky junction produced by the Au-TiO_2 interaction [38]. Comparing Au/TiO_2 and Au/TiO_2-SMSI, the band gap also changed decreasing to 3.07 eV, this new reduction can be explained by a greater Au-TiO_2 interaction due to a higher Au-TiO_2 contact.

The three samples exhibited very similar survey XPS spectra, showing the titanium and oxygen signals corresponding to TiO_2 (Fig. 3) and the characteristic adventitious carbon contamination peak, the only most remarkable difference was the presence of weak gold signals from the AuNPs for Au/TiO_2 and Au/TiO_2-SMSI photocatalysts. The atomic compositions obtained from these spectra (Table 2) determined O:Ti ratios of 2.3, 2.4 and 2.2 for TiO_2, Au/TiO_2 and Au/TiO_2-SMSI, respectively. These deviations from the TiO_2 stoichiometry are due to the contribution of O 1 s signal associated to surface hydroxyl groups [39], thus, the observed differences can be related to changes in the OH surface density. If the OH contribution is omitted, the O/Ti ratio for all samples becomes 2 indicating that the synthetic procedure did not produce substantial changes in the TiO_2 oxidation state. The gold contents (equivalent to 5 and 4 wt%) were higher than those determined by ICP-AES. This variation is common for this type of photocatalysts [40] due to the surface sensitivity of the XPS, which overestimates the Au signal of AuNPs located in the TiO_2 outer surface. The lower gold content of Au/TiO_2-SMSI can be also associated with the surface sensitivity of the technique because the covering of AuNPs with a TiO_2 layer may reduce the gold signal intensity. The Ti 2p high resolution spectra of the photocatalysts (Fig. 3) were composed by two peaks corresponding to $2p_{3/2}$ and $2p_{1/2}$ levels at around 458.5 and 464 eV, respectively, whose separation was 5.7 eV. The exact position of Ti $2p_{3/2}$ peaks are presented in Table 2. The bare TiO_2 showed a value in accordance with the bibliography [41], but slight shifts were observed for Au/TiO_2 and Au/TiO_2-SMSI. The shift to higher binding energies for Au/TiO_2 suggest that Ti atoms have a lower electron density due to electron transference from TiO_2 to AuNPs [42–45]. The difference in the work function of TiO_2 (4.0–4.7 eV for anatase [46,47]) and Au (5.1 eV [48]) produces an electron migration from TiO_2 to AuNPs until the equilibration of Fermi levels [49]. In the case of the Au/TiO_2-SMSI sample, this peak was shifted to lower binding energies in comparison with Au/TiO_2 and this might be related to a less oxidized titanium. Indeed, an additional small peak can be found at 456.56 eV for Au/TiO_2-SMSI, a position close to the tabulated value for Ti^{3+} (457.1 eV [50]). This feature suggests that the produced overlayer contained a significant amount of Ti^{3+} atoms due to the incomplete oxidation of Ti^{3+} precursor. The detection of Ti^{3+} state allows to distinguish between SMSI and a simple massive coverage with titania, since the formation of a partially reduced support overlayer on metal nanoparticles is one of the identifying features of classical SMSI [51]. According to this finding the formed overlayer will be hereinafter denoted as TiO_x. The O 1 s spectra can be fitted by two components, a main peak centred close to 530 eV attributed to oxygen atoms in the TiO_2 lattice and a small peak at higher energies that corresponds to the surface hydroxyl groups of TiO_2 [52]. The oxygen main peak was shifted following the same trend observed for Ti $2p_{3/2}$ peak (Table 2) and even an additional peak related to oxygen bonded to Ti^{3+} can be also observed for Au/TiO_2-SMSI. Regarding the hydroxyl peak, its intensity was considerably higher for Au/TiO_2 being 0.19 its area ratio with respect to the main peak and 0.12 for the other samples. This seems to confirm a higher presence of hydroxyl groups in Au/TiO_2. The Au 4 f core level exhibited two peaks from the Au 4 $f_{7/2}$ and 4 $f_{5/2}$ signals that were positioned in binding energy values lower than 84 eV, the tabulated value for bulk gold (Table 2) [41]. A negative shift implies a higher electron density in the atoms, which confirms the electron transfer from TiO_2 to AuNPs [53]. The higher work function of Au (5.1 eV [48]) causes the electron movement from TiO_2 (4.0–4.7 eV for anatase [46,47]) to AuNPs until the Fermi levels equilibration [49]. This shift was higher for Au/TiO_2-SMSI revealing a higher electron transference associated to the AuNPs covered by TiO_x that increases the gold-titania interphase and the consequent interaction. Regarding the valence band spectra (Fig. 3), TiO_2 showed the valence band edge at 2.6 eV and slightly decreased to 2.4 eV for the Au/TiO_2 and Au/TiO_2-SMSI photocatalysts. Additionally, these photocatalysts exhibited higher electron population at low binding energies which can be related to gold energy levels associated to its 5d band [39].

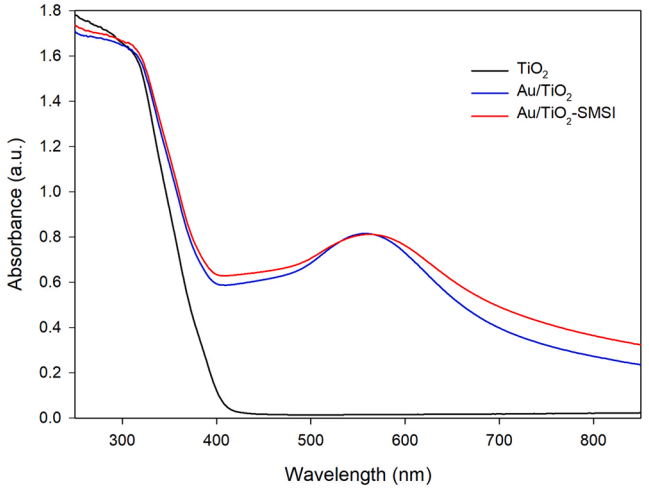

Fig. 2. UV–Visible spectra of the studied photocatalysts.

TEM becomes an essential technique in order to detect TiO_x overlayers covering the AuNPs. In our case, the bare TiO_2 was formed by angular nanoparticles with sizes around 25 nm and less abundant particles with bigger sizes (Fig. 4a). This structure corresponds to the characteristic morphology of P25 photocatalyst, where the small particles are identified as anatase and the bigger ones as rutile [54]. Both gold containing photocatalysts showed essentially the same structure (Fig. 4b and c) since the employed synthesis conditions were too soft to induce changes in the TiO_2 morphology [55]. The AuNPs were easily identified in these photocatalysts due to their darker contrast. A closer view of AuNPs allowed to observe their structure denoting differences between Au/TiO_2 and Au/TiO_2-SMSI photocatalyts. Au/TiO_2 showed particles with well-defined edges (Fig. 4d) whereas the AuNPs of Au/TiO_2-SMSI were enveloped by a thin layer that emerged from the support (Fig. 4e and f). The same change has been observed for Au/TiO_2 catalysts when a classical SMSI geometrical effect is induced [56], which confirms that

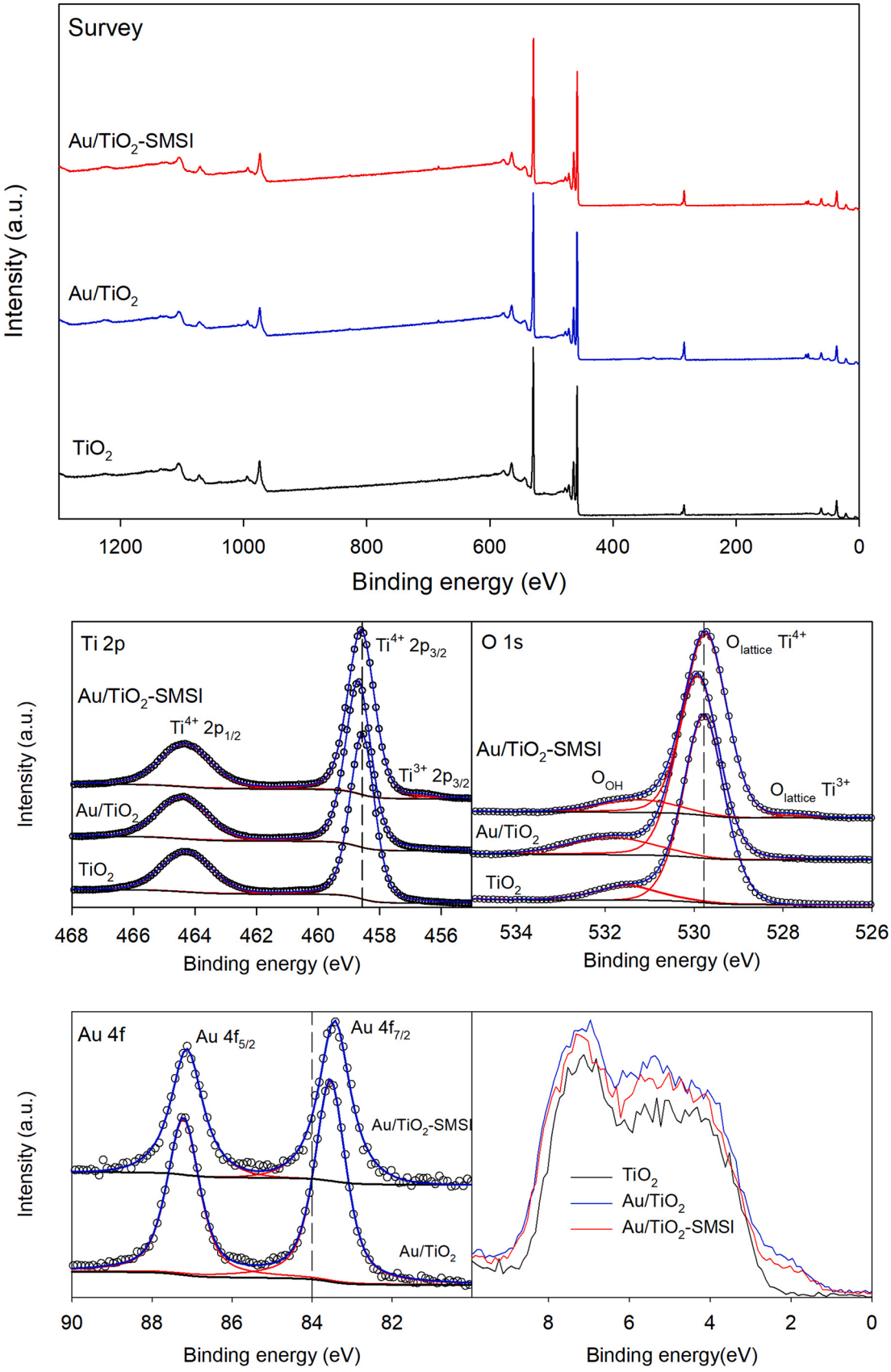

Fig. 3. Survey XPS (top), high resolution XPS and valence band spectra (bottom right) obtained for the photocatalysts under study.

Table 2
Results of XPS characterization.

		TiO_2	Au/TiO_2	Au/TiO_2-SMSI
Concentration (at%)	Ti	30.71	29.04	31.06
	O	69.29	70.21	68.44
	Au	-	0.75	0.50
Peak Energy (eV)	Ti $2p_{3/2}$	458.57	458.65	458.60
	O 1 s	529.78	529.92	529.74
	Au 4 $f_{7/2}$	-	83.54	83.46
Chemical shift (eV)*	Ti $2p_{3/2}$	-	0.08	0.03
	O 1 s	-	0.14	-0.04
	Au 4 $f_{7/2}$	-	-0.46	-0.56

* Chemical shifts for Ti 2p3/2 and O 1 s calculated from TiO_2 sample values, for Au 4f7/2 the reference value (84 eV) was employed.

the wet-chemistry method employed effectively induced a SMSI effect in the Au/TiO_2 photocatalyst. The elemental mapping using the STEM-HAADF technique (Fig. 4g) allowed confirming the presence of titanium on AuNPs providing another evidence about the formation of TiO_x overlayers.

The change in AuNPs size distribution after SMSI induction was determined from HAADF-STEM images where the difference in contrast between gold and titanium phases is sharpened. The Au/TiO_2 presented AuNPs with sizes ranging from 1.5 to 7 nm being their average size 3.1 $\pm$ 1.0 nm (Fig. 5a). On the other hand, Au/TiO_2-SMSI displayed a fraction of particles higher in size (Fig. 5b), widening its particle size distribution and extending the upper size limit until nearly 10 nm, with an average size of 3.8 $\pm$ 1.7 nm. Similar growth of AuNPs was observed for Au/TiO_2 catalysts prepared employing the same procedure as ours to achieve the SMSI effect [19]. It should be noted that temperatures as higher as 600 ºC under a reducing atmosphere are required for inducing the SMSI interaction on AuNPs sizes around 3 nm employing the classical procedure in the Au/TiO_2 system [56]. In addition to more severe gold sintering effects, these high temperatures can also modify the structure of TiO_2 support having a significant impact on photoactivity [57]. In this way, it is confirmed that the employed soft methodology allows obtaining SMSI effects in titania-based photocatalysts with a reduced impact on their structure.

The suppression of chemisorption of small molecules such as H_2 and CO onto the surface of the metal supported nanoparticles is one of the characteristics of a classical SMSI state [13]. This feature was

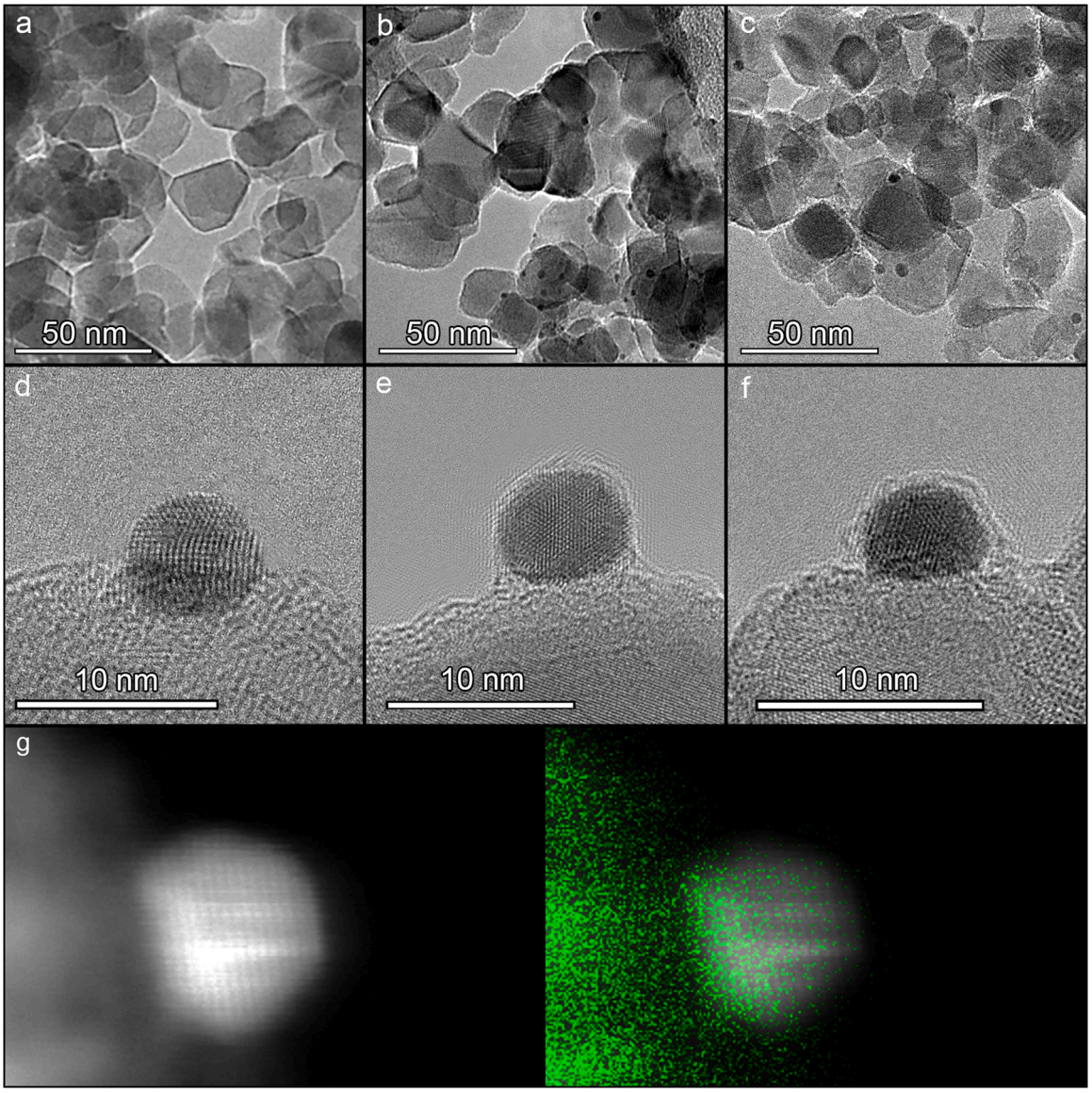

Fig. 4. TEM and HRTEM images of TiO_2 (a), Au/TiO_2 (b and d) and Au/TiO_2-SMSI (c, e and f) photocatalysts. STEM-HAADF image of the Au/TiO_2-SMSI sample and the corresponding Ti (green) elemental map (g).

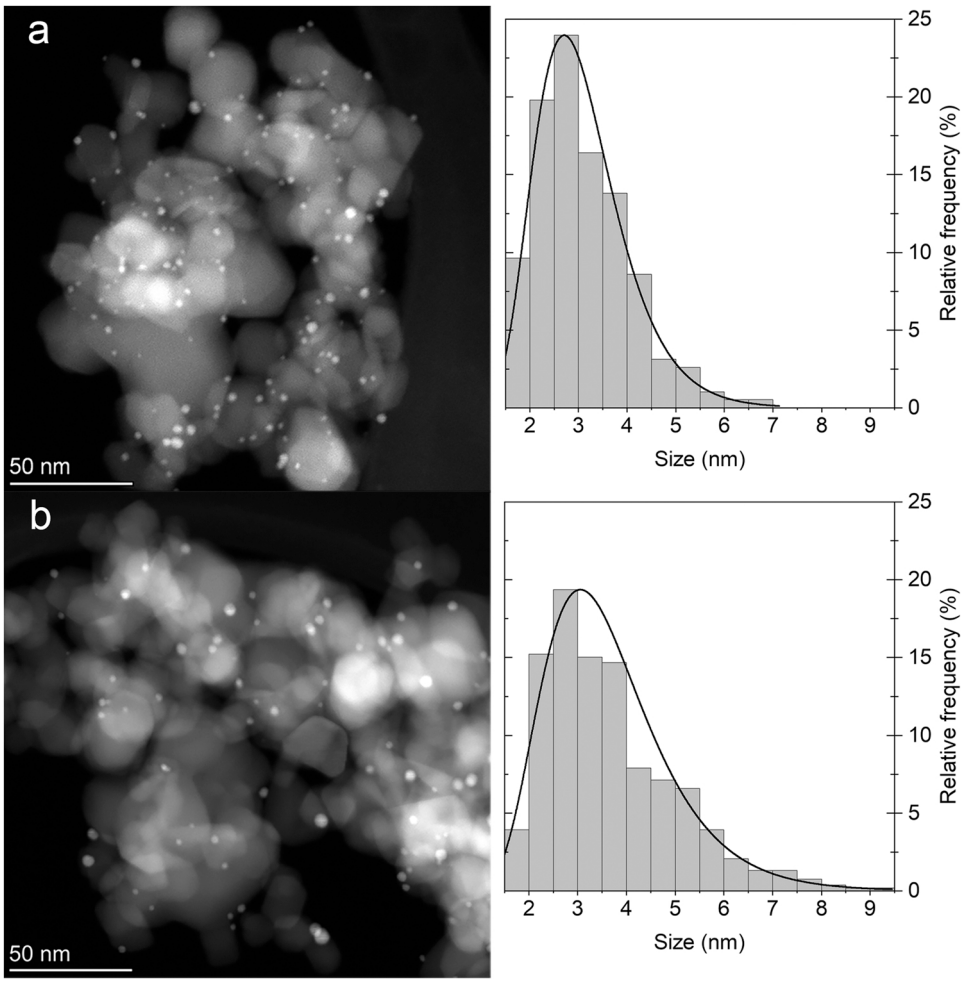

Fig. 5. Representative STEM-HAADF images and AuNPs size distributions obtained for Au/TiO_2 (a) and Au/TiO_2-SMSI (b) photocatalysts.

investigated by CO chemisorption measurements and the corresponding isotherms are showed in Fig. 6. The CO adsorption on Au/TiO_2 was significantly higher than that obtained on bare TiO_2, so we can attribute the excess to CO adsorbed onto the AuNPs surface. As expected, the AuNPs coverage with the TiO_x overlayer partially blocked the CO adsorption on the gold surface thus decreasing the amount of CO adsorbed. Specifically, the amount of CO adsorbed on gold was reduced by half for Au/TiO_2-SMSI with respect to the starting photocatalyst (from 0.39 to 0.19 expressed in CO/Au apparent ratio, Table 1). This decrease cannot be justified by the slight difference of AuNPs sizes between both samples confirming that this effect was mainly due to the TiO_x covering of gold atoms.

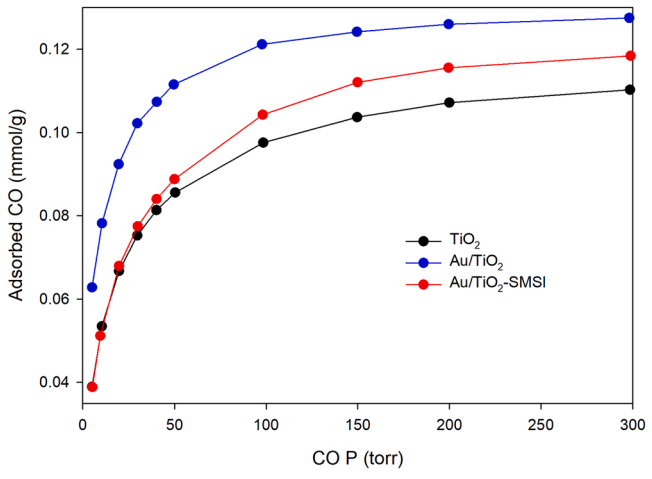

Fig. 6. Second CO adsorption isotherms obtained for the photocatalysts under study.

3.2. *Photoactivity evaluation*

The activity of the photocatalysts was evaluated by means of methylene blue (MB) degradation tests under UV and UV-Vis radiation, being this molecule a standard model for studying the performance of the photocatalysts for water pollutants removal. The evolution of MB absorbance solution is illustrated in Fig. 7 and the corresponding reaction rate constants for a first order kinetic fitting are compiled in Table 3. Under UV light, both gold containing photocatalysts showed less activity than bare TiO_2, which can be related to its higher tendency to particle aggregation observed by DLS that reduces the photocatalyst effective area. Comparing Au/TiO_2 and Au/TiO_2-SMSI, the MB degradation was higher when SMSI effect is present in the photocatalyst, because the TiO_2-Au contact creates a Schottky junction that decreases the electron-hole recombination rate [58] and the AuNPs coverage promotes this interaction. Furthermore, the TiO_{2-x} layer can also promote the photoactivity due to the Ti^{3+} states that can act as electron traps preventing the recombination [59]. The differences between the samples were more significant when UV-Vis light was employed. No improvement in MB degradation was observed for TiO_2 since the contribution of new wavelengths corresponding to visible range cannot be absorbed by TiO_2. On the other hand, the MB degradation for Au/TiO_2 slightly promoted

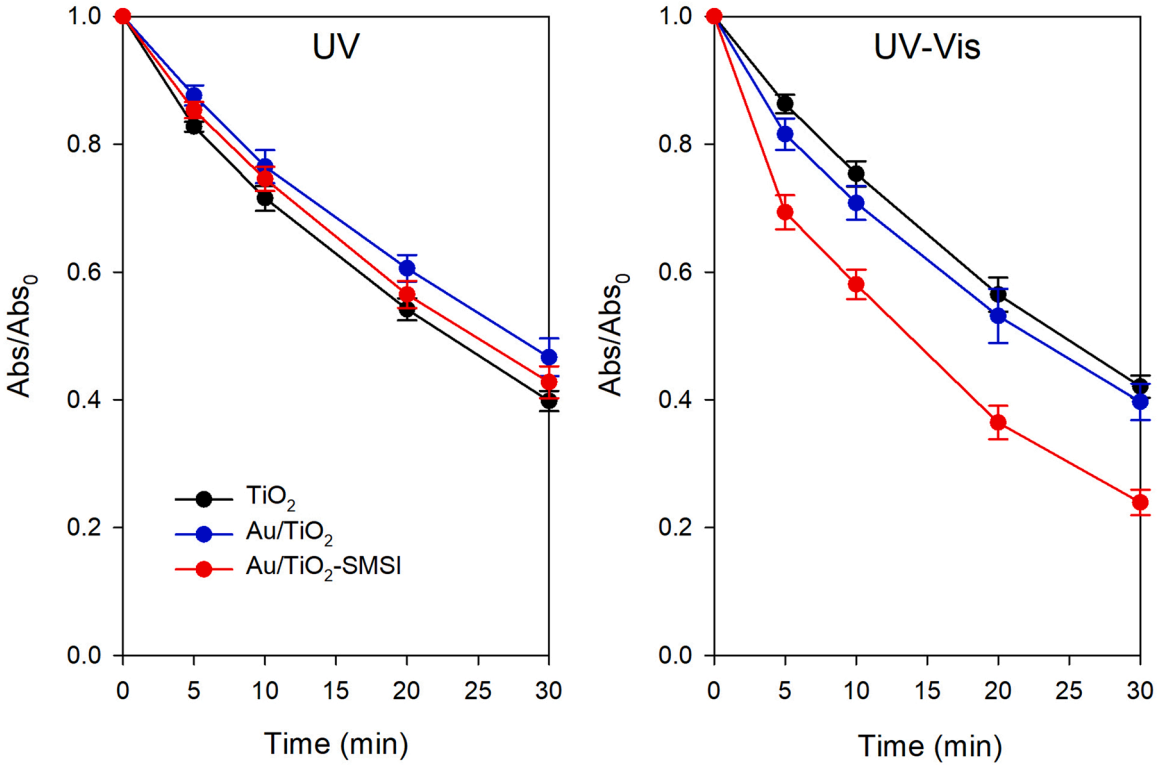

Fig. 7. MB solution absorbance evolution during the photodegradation tests under UV or UV–Vis radiation.

Table 3
Rate constants obtained from the first order fitting for MB and soot degradation results.

Photocatalyst	Reaction rate constant		
	MB UV (min^{-1})	MB UV-Vis (min^{-1})	Soot (d^{-1})
TiO_2	0.030	0.029	0.08
Au/TiO_2	0.025	0.030	0.15
Au/TiO_2-SMSI	0.028	0.046	0.24

because visible light can be absorbed by the AuNPs due to LSPR effect and the excited electrons can be injected to the conduction band of TiO_2 triggering the formation of radicals responsible for the MB degradation [60]. The MB degradation for Au/TiO_2-SMSI under UV–vis light was considerably promoted showing a reaction rate 50% higher than that of all other experiments. This better performance of the photocatalyst with SMSI effect can be attributed to the combination of two factors: (1) the plasmonic effect is promoted due to the formation of the new interface contact Au-TiO_{2-x} overlay [18] and (2) the presence of oxygen vacancies in the TiO_{2-x} interface also increases the LSPR effect and promotes the electron transference [61]. Therefore, considering the results, this type of photocatalytic processes where the photocatalysts are dispersed in water must be carried out at pH values that ensure the proper photocatalyst dispersion.

Another key scenario for photocatalytic environmental applications is the removal of gaseous pollutants, this characteristic was evaluated by means of NO abatement. The evolution in the NO, NO_2 and NO_x concentration during the photooxidation tests are plotted in Fig. 8. The results considering the total irradiation time are presented in Fig. 9 which shows the amount of NO converted, NO_x removed and NO_2 generated expressed as percentage with respect to the total amount NO and also the selectivity percentage of the process towards NO_2 formation. Once irradiation started, the NO concentration dropped immediately after the sample irradiation started and recovered the initial concentration when the irradiation finished, confirming the photoactivity of the samples. All samples reached similar NO levels that remained almost stable during the irradiation period, probably this is the maximum NO conversion that can be achieved under these experimental settings. However, obvious differences in NO_2 concentrations were observed being the released amounts far lower for the gold containing photocatalysts. This resulted in the increase of total NO_x elimination and lower selectivity towards NO_2. This trend in selectivity is especially desirable due to the fact that NO_2 is more toxic than NO and an excessive release of NO_2 can increase the harmfulness of the air rather than mitigate it [29]. Therefore, the $DeNO_x$ index (Fig. 9), which considers the NO conversion and the NO_2 release, is a better way for comparing the NO_x depolluting potential of the photocatalysts. In this way, the $DeNO_x$ index for Au/TiO_2 and Au/TiO_2-SMSI photocatalysts was approximately 3.5 times the value corresponding to TiO_2, emphasizing the effect of AuNPs.

This better performance is not only because AuNPs promote the TiO_2 photoactivity improvement but also it has been reported that AuNPs have a role in the NO oxidation process adsorbing O_2 and NO on their surface [45,62]. Additionally, the NO_2 molecule can be also adsorbed and activated by gold [63]. These effects can explain the great change in the selectivity when AuNPs are deposited on TiO_2. Comparing Au/TiO_2 and Au/TiO_2-SMSI, the SMSI effect did not add any benefit and their results are even slightly worse than those corresponding to Au/TiO_2. Despite the SMSI effect promotes the photoactivity of Au/TiO_2 photocatalyst, it also blocks the adsorption of gas molecules, as demonstrated by CO chemisorption experiments. This loss of gold adsorption capacity can also affect how the gas molecules involved in the NO photooxidation process react. In this sense, the NO and NO_2 molecules can be strongly adsorbed on AuNPs surface being activated and facilitating their reaction with the radicals generated in the photocatalyst surface. If Au adsorption sites are covered by the TiO_x, the radicals react with weakly adsorbed molecules (non-activated) or they need diffusing to the gas phase to interact with non-adsorbed molecules. In this way, the potential benefits of the SMSI state are counterbalanced by the loss of adsorption capacity of the gold phase. On this basis, if the mechanism of the

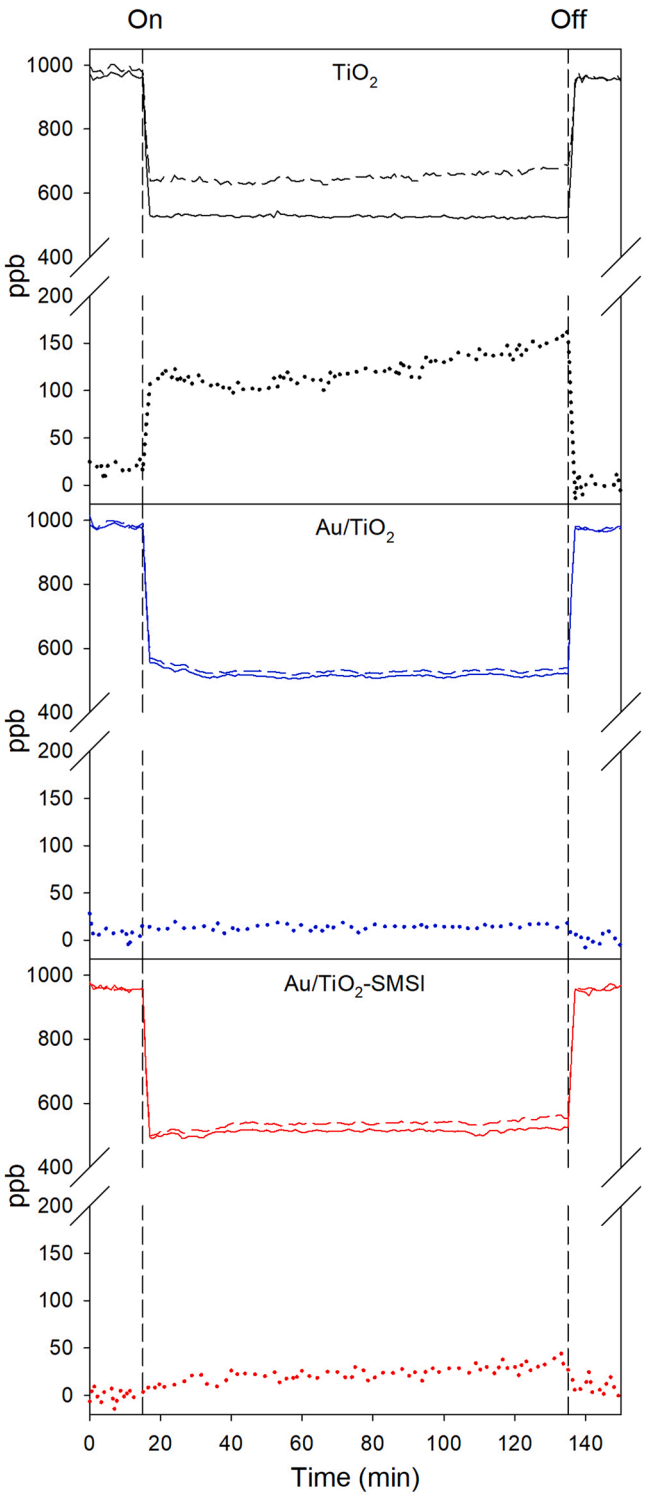

Fig. 8. NO (solid), NO_2 (dotted) and NO_x (dashed) concentration profiles during NO photooxidation tests.

photocatalytic process requires the adsorption of species on gold, the SMSI geometrical effect would be not recommended. Instead, a partial encapsulation of the AuNPs or the formation of a porous TiO_x overlayer that would allow the adsorption on gold should be explored in these cases.

Finally, here we present the results of the photodegradation of pollutants directly deposited on the photocatalysts. This situation is of particular interest to applications related to self-cleaning surfaces but it

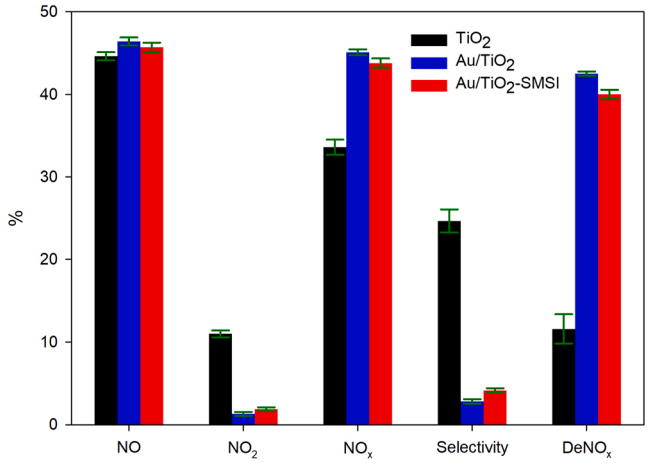

Fig. 9. Results of NO photooxidation tests.

is also relevant to every photocatalytic application since the accumulation of organic matter on the photocatalysts can deactivate them. Soot was chosen because it is a common pollutant associated with combustion processes, it is difficult to remove and its deposition produces dark stains that limit the radiation received by the photocatalyst. Fig. 10 shows the evolution of a soot layer deposited on glass plates coated with the photocatalysts under study at different irradiation times. SiO_2 coated samples were also prepared in order to confirm that the soot elimination was due to TiO_2 photoactivity rather than other effects such as photolysis. The soot layer on SiO_2 remained unaltered after 14 days of irradiation, the slight disappearance of soot colour around the plate edges corresponds to the mechanical removal of soot during the sample manipulation to perform the measurements. On the contrary, soot deposited on TiO_2 gradually disappeared from the ends to the centre of the plate, which is related to the carbon photomineralization to CO_2 by TiO_2 [64]. The non-homogeneous degradation pattern observed can be related to the soot deposition method employed, the centre of the samples was placed over the flame producing a thicker soot layer in that area. Soot degradation was significantly faster in Au/TiO_2 sample being the stain almost totally eliminated after 14 days of irradiation whereas a considerable fraction of the stain remained in the TiO_2 sample. Au/TiO_2-SMSI showed the highest degradation rate achieving in only 10 days a soot elimination similar to that observed for Au/TiO_2 at the end of the performed tests.

A deeper analysis of the soot degradation based on the measurement of the soot layer absorbance was performed in order to obtain quantitative results about its elimination. The soot degradation curves obtained from these absorbance measurements are shown in Fig. 11. The obtained results are in accordance with the visual inspection of the photographs, showing the same trend with no elimination for SiO_2 sample and an increasing degradation rate in the order $TiO_2 < Au/TiO_2 < Au/TiO_2$-SMSI. Mills et al. suggested that the results of this type of soot photodegradation approximate a first order kinetics [64], but more complex models are required to get a good fitting [65]. However, the present results fitted very well to a first order kinetics ($R^2 > 0.99$) providing the rate constants compiled in Table 3. This discrepancy can be attributed to the different methodologies employed for determining the soot degradation. Mills et al. measured the amount of CO_2 released and this method considers the soot elimination in the whole sample. Since there were areas where soot elimination was faster than other, due to the inhomogeneous soot deposition, the kinetics of CO_2 release would be a combination of the different kinetics in each sample area. Despite the samples in this work also exhibited a non-homogeneous soot elimination, each absorbance measurement was made in the same point of the sample presenting a more consistent kinetics during the entire test. In any case, our results revealed that the soot degradation rate was

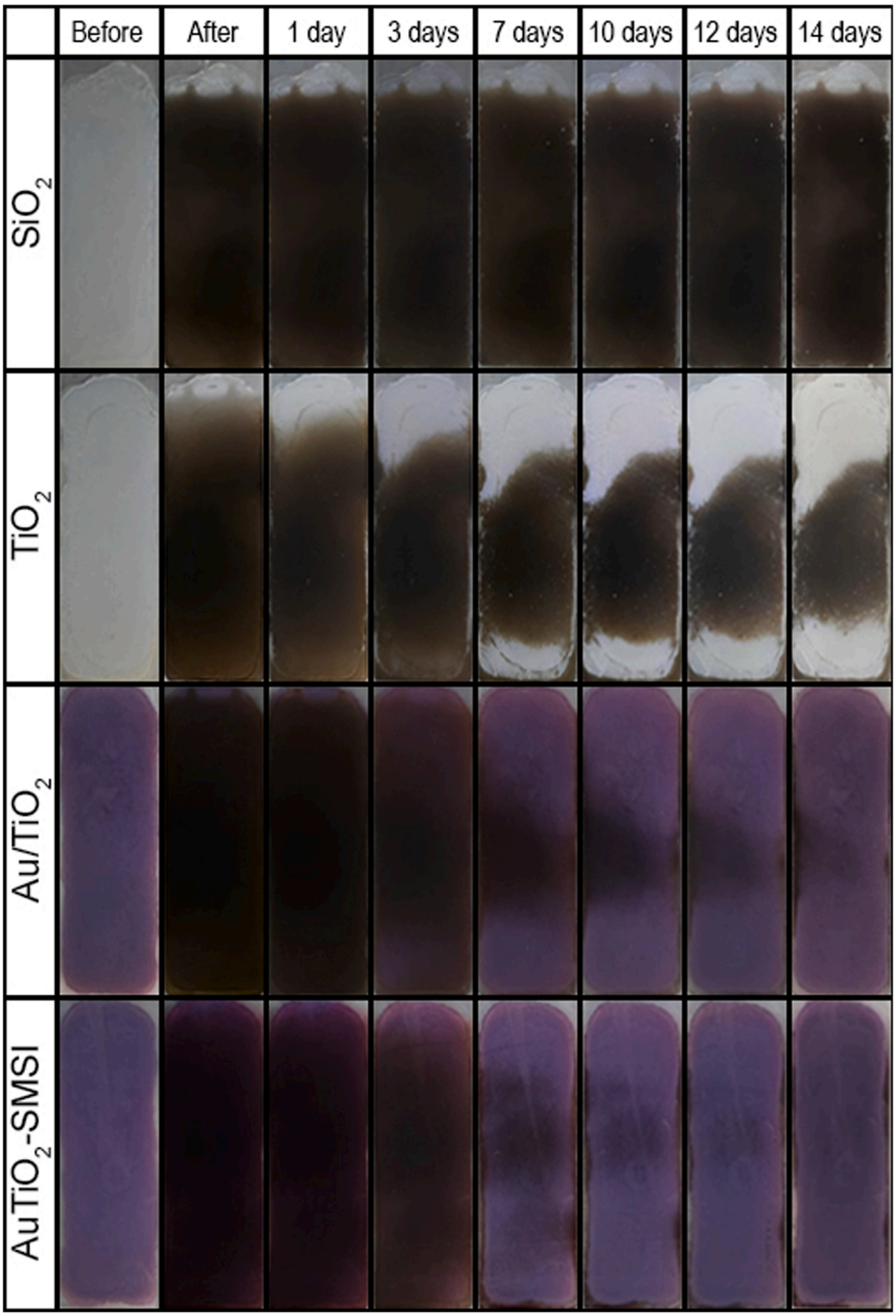

Fig. 10. Evolution of soot stains during the UV-Vis irradiation.

nearly doubled for the Au/TiO_2 photocatalyst. The hydroxyl radical is the main oxidizing agent responsible for degrading soot, being the migration of these radicals from TiO_2 surface to soot the dominant mechanism [30]. The higher lifetime of photogenerated holes in Au/TiO_2 due to the Schottky junction promotes the generation of $^{\bullet}OH$ radicals [58], explaining their higher activity. In addition, Au/TiO_2 photocatalysts are able to produce $^{\bullet}OH$ radicals after the AuNPs excitation and the electron injection to TiO_2 conduction band under visible light [66]. For its part, Au/TiO_2-SMSI increased the degradation rate by 60% confirming that SMSI effect promotes the processes where the degradation mechanism happens through the formation of reactive oxygen species. As mentioned earlier, the SMSI state intensifies the mechanisms that promote the photoactivity in Au/TiO_2 photocatalyst and, additionally, the presence of Ti^{3+} defects in the TiO_{2-x} overlayer also promote the formation of $^{\bullet}OH$ radicals [67]. Because the photocatalyst was immobilized and soot did not have to interact directly with Au surface, the drawbacks associated with Au/TiO_2-SMSI photocatalyst observed in the previous processes do not have impact on this reaction.

4. Conclusions

A Strong Metal-Support Interaction (SMSI) was induced in Au/TiO_2 photocatalysts using a wet chemistry, non-conventional, soft method in order to evaluate its impact on photocatalytic activity excluding side

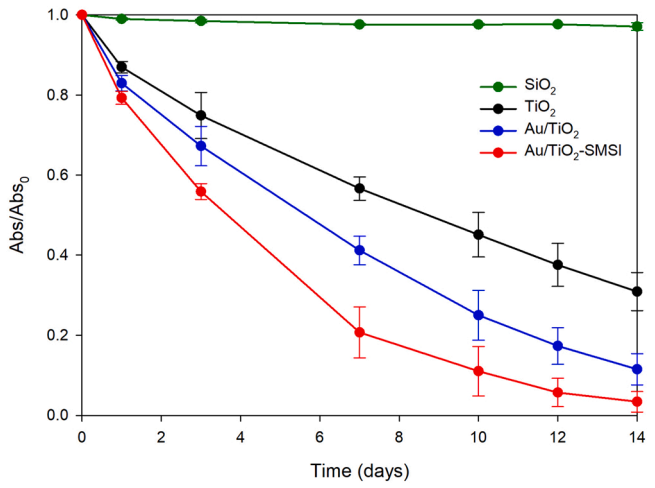

Fig. 11. Soot degradation curves corresponding to the photodegradation test.

effects related to the use of thermal treatments at elevated temperatures. The characterization of the photocatalysts confirmed that the effective covering of the gold nanoparticles (AuNPs) was produced without detectable changes in the titania support. The XPS revealed that the SMSI induced the photocatalyst showed shifts in their core levels and the presence of Ti^{3+} while HRTEM and compositional STEM mapping allowed detecting TiO_x covering the AuNPs. As expected, the capacity of the gold phase to adsorb gaseous molecules such as CO was significantly limited.

The photocatalytic properties were deeply evaluated under three different photooxidation scenarios that are representative examples of real photocatalytic environmental applications. The solid-water process, typical application related to elimination of water pollutants, was evaluated by the photodegradation of MB under UV and UV–vis radiation. In both cases, the Au/TiO_2 photocatalyst under SMSI state showed higher MB elimination than Au/TiO_2, especially under UV–vis light with an increase of over 50%. The solid-air process is associated with atmospheric pollutants removal and it was evaluated by means of NO photooxidation. Despite AuNPs considerably promoted the NO_x elimination of TiO_2, the SMSI did not provide additional benefits, being the results even slightly worse. This was attributed to the coverage of AuNPs with the TiO_x overlayer that hinders the adsorption of molecules onto the gold surface. The solid-solid reaction represents the elimination of pollutants deposited on a photocatalytic coating, which is linked to self-cleaning application and it was studied by soot photodegradation. In this case, the SMSI revealed the highest photoactivity enhancement, increasing the soot photoelimination rate of Au/TiO_2 by 60% and it was tripled compared to TiO_2.

As a final remark, despite the SMSI in Au/TiO_2 photocatalysts has a positive impact on photoactivity, it can also promote certain side effects that may limit the real depolluting effectiveness under specific scenarios. Specifically, we have detected changes in the acid-base behaviour of the photocatalyst and a loss of NOx adsorption capacity by gold. These side effects must be taken into consideration depending on the type of photocatalytic application to make the appropriate optimizations that avoid an activity loss. For example, for the cases studied in this work, a pH that ensure the proper photocatalyst dispersion must be employed for water applications and a partial AuNPs coverage must be considered if the reaction mechanism require adsorption of the involved species on Au surface.

CRediT authorship contribution statement

Manuel Luna: Conceptualization, Investigation, Writing – original draft. **Adrian Gonzalez-Hidalgo:** Investigation. **Ana Diaz:** Investigation. **Daniel Goma:** Investigation. **José Manuel Gatica:** Conceptualization, Writing – review & editing, Supervision, Funding acquisition **María Jesús Mosquera:** Conceptualization, Funding acquisition.

Declaration of Competing Interest

The authors declare that they have no known competing financial interests or personal relationships that could have appeared to influence the work reported in this paper.

Data Availability

Data will be made available on request.

Acknowledgments

This work has been supported by the Ministry of Science and Innovation of Spain/FEDER Programme of the EU (PID2020-115843RB-I00/AEI/10.13039/501100011033) and cofinancied by the European Union under the 2014-2020 ERDF Operational Programme and by the Department of Economic Transformation, Industry, Knowledge, and Universities of the Regional Government of Andalusia (FEDER-UCA18-106613). The University Institute of Research on Electron Microscopy and Materials (IMEYMAT) of Cadiz University (NANOforCOAT Project) and the Junta de Andalucía (FQM-110 group) also supported the investigation. M. Luna thanks the Spanish Government for his Margarita Salas grant (2021-067/PN/MS-RECUAL/CD) supported by the European Union-NextGenerationEU.

Appendix A. Supporting information

Supplementary data associated with this article can be found in the online version at doi:10.1016/j.jece.2023.109947.

References

[1] T.W. van Deelen, C. Hernández Mejía, K.P. de Jong, Control of metal-support interactions in heterogeneous catalysts to enhance activity and selectivity, Nat. Catal. 2 (2019) 955–970, https://doi.org/10.1038/s41929-019-0364-x.
[2] X. Liu, J. Iocozzia, Y. Wang, X. Cui, Y. Chen, S. Zhao, Z. Li, Z. Lin, Noble metal-metal oxide nanohybrids with tailored nanostructures for efficient solar energy conversion, photocatalysis and environmental remediation, Energy Environ. Sci. 10 (2017) 402–434, https://doi.org/10.1039/c6ee02265k.
[3] D.A. Panayotov, J.R. Morris, Surface chemistry of Au/TiO_2: thermally and photolytically activated reactions, Surf. Sci. Rep. 71 (2016) 77–271, https://doi.org/10.1016/j.surfrep.2016.01.002.
[4] V. Subramanian, E.E. Wolf, P.V. Kamat, Catalysis with TiO_2/gold manocomposites. Effect of metal particle size on the fermi level equilibration, J. Am. Chem. Soc. 126 (2004) 4943–4950, https://doi.org/10.1021/ja0315199.
[5] L. Lin, Q. Zhong, Y. Zheng, Y. Cheng, R. Qi, R. Huang, Size effect of Au nanoparticles in Au-TiO_{2-x} photocatalyst, Chem. Phys. Lett. 770 (2021), https://doi.org/10.1016/j.cplett.2021.138457.
[6] A. Khan, A. Adam, M.A. Aziz, M.I. Ahmed, Z.H. Yamani, M. Qamar, Shape-dependent performance of gold nanocrystals supported on TiO_2 for photoelectrochemical water oxidation under different radiations, Int. J. Hydrog. Energy 44 (2019) 23054–23065, https://doi.org/10.1016/j.ijhydene.2019.07.062.
[7] Z. Cao, Y. Yin, P. Fu, D. Li, Y. Zhou, Z. Wen, Y. Peng, W. Wang, W. Zhou, D. Tang, Branched TiO_2 nanorod arrays decorated with Au nanostructure for plasmon-enhanced photoelectrochemical water splitting, J. Electrochem. Soc. 167 (2020), 026509, https://doi.org/10.1149/1945-7111/ab6a7c.
[8] S.J. Tauster, S.C. Fung, R.L. Garten, Strong metal-support interactions. Group 8 noble metals supported on titanium dioxide, J. Am. Chem. Soc. 100 (1978) 170–175, https://doi.org/10.1021/ja00469a029.
[9] S.J. Tauster, Strong metal-support interactions, Acc. Chem. Res. 20 (1987) 389–394, https://doi.org/10.1021/ar00143a001.
[10] S. Roberts, R.J. Gorte, A study of the migration and stability of titania on a model Rh catalyst, J. Catal. 124 (1990) 553–556, https://doi.org/10.1016/0021-9517(90)90202-U.
[11] Z. Luo, G. Zhao, H. Pan, W. Sun, Strong Metal–Support Interaction in heterogeneous catalysts, Adv. Energy Mater. 12 (2022) 2201395, https://doi.org/10.1002/aenm.202201395.
[12] X. Liu, M.H. Liu, Y.C. Luo, C.Y. Mou, S.D. Lin, H. Cheng, J.M. Chen, J.F. Lee, T. S. Lin, Strong metal-support interactions between gold nanoparticles and ZnO

nanorods in CO oxidation, J. Am. Chem. Soc. 134 (2012) 10251–10258, https://doi.org/10.1021/ja3033235.
[13] H. Tang, Y. Su, B. Zhang, A.F. Lee, M.A. Isaacs, K. Wilson, L. Li, Y. Ren, J. Huang, M. Haruta, B. Qiao, X. Liu, C. Jin, D. Su, J. Wang, T. Zhang, Classical strong metal–support interactions between gold nanoparticles and titanium dioxide, Sci. Adv. 3 (2017) 1–8, https://doi.org/10.1126/sciadv.1700231.
[14] X.F. Wu, H.Y. Song, J.M. Yoon, Y.T. Yu, Y.F. Chen, Synthesis of core-shell Au@TiO_2 nanopartides with truncated wedge-shaped morphology and their photocatalytic properties, Langmuir 25 (2009) 6438–6447, https://doi.org/10.1021/la900035a.
[15] J.C. Colmenares, A. Magdziarz, M.A. Aramendia, A. Marinas, J.M. Marinas, F. J. Urbano, J.A. Navio, Influence of the strong metal support interaction effect (SMSI) of Pt/TiO_2 and Pd/TiO_2 systems in the photocatalytic biohydrogen production from glucose solution, Catal. Commun. 16 (2011) 1–6, https://doi.org/10.1016/j.catcom.2011.09.003.
[16] Q. Li, K. Wang, S. Zhang, M. Zhang, J. Yang, Z. Jin, Effect of photocatalytic activity of CO oxidation on Pt/TiO_2 by strong interaction between Pt and TiO_2 under oxidizing atmosphere, J. Mol. Catal. A Chem. 258 (2006) 83–88, https://doi.org/10.1016/j.molcata.2006.05.030.
[17] C.H. Lin, J.H. Chao, C.H. Liu, J.C. Chang, F.C. Wang, Effect of calcination temperature on the structure of a Pt/TiO_2 (B) nanofiber and its photocatalytic activity in generating H_2, Langmuir 24 (2008) 9907–9915, https://doi.org/10.1021/la800572g.
[18] W. Zhang, X. Li, S. Liu, J. Qiu, J. An, J. Yao, S. Zuo, B. Zhang, H. Xia, C. Li, Photocatalytic oxidation of 5–hydroxymethylfurfural over interfacial-enhanced Ag/TiO2 under visible light irradiation, ChemSusChem 15 (2022), e202102158, https://doi.org/10.1002/cssc.202102158.
[19] J. Zhang, H. Wang, L. Wang, S. Ali, C. Wang, L. Wang, X. Meng, B. Li, D.S. Su, F. S. Xiao, Wet-chemistry strong metal-support interactions in titania-supported au catalysts, J. Am. Chem. Soc. 141 (2019) 2975–2983, https://doi.org/10.1021/jacs.8b10864.
[20] G. Wang, L. Xu, J. Zhang, T. Yin, D. Han, Enhanced photocatalytic activity of powders (P25) via calcination treatment, Int. J. Photo 2012 (2012) 1–9, https://doi.org/10.1155/2012/265760.
[21] K. Lv, Q. Xiang, J. Yu, Effect of calcination temperature on morphology and photocatalytic activity of anatase TiO_2 nanosheets with exposed {001} facets, Appl. Catal. B Environ. 104 (2011) 275–281, https://doi.org/10.1016/j.apcatb.2011.03.019.
[22] H. Petrova, J.P. Juste, I. Pastoriza-Santos, G.V. Hartland, L.M. Liz-Marzán, P. Mulvaney, On the temperature stability of gold nanorods: comparison between thermal and ultrafast laser-induced heating, Phys. Chem. Chem. Phys. 8 (2006) 814–821, https://doi.org/10.1039/b514644e.
[23] M. Haruta, Size- and support-dependency in the catalysis of gold, Catal. Today 36 (1997) 153–166, https://doi.org/10.1016/S0920-5861(96)00208-8.
[24] J. Tauc, Optical properties and electronic structure of amorphous Ge and Si, Mater. Res. Bull. 3 (1968) 37–46, https://doi.org/10.1016/0025-5408(68)90023-8.
[25] S.P. Tandon, J.P. Gupta, Measurement of forbidden energy gap of semiconductors by diffuse reflectance technique, Phys. Status Solidi 38 (1970) 363–367, https://doi.org/10.1002/pssb.19700380136.
[26] J.M. Gatica, R.T. Baker, P. Fornasiero, S. Bernal, J. Kašpar, Characterization of the metal phase in NM/$Ce_{0.68}Zr_{0.32}O_2$ (NM: Pt and Pd) catalysts by hydrogen chemisorption and HRTEM microscopy: a comparative study, J. Phys. Chem. B 105 (2001) 1191–1199, https://doi.org/10.1021/jp003632g.
[27] M. López-Haro, J.M. Cíes, S. Trasobares, J.A. Pérez-Omil, J.J. Delgado, S. Bernal, P. Bayle-Guillemaud, O. Stéphan, K. Yoshida, E.D. Boyes, P.L. Gai, J.J. Calvino, Imaging nanostructural modifications induced by electronic metal−support interaction effects at Au||cerium-based oxide nanointerfaces, ACS Nano 6 (2012) 6812–6820, https://doi.org/10.1021/nn301557u.
[28] ISO 22197–1: 2016; Fine ceramics (advanced ceramics, advanced technical ceramics) – Test method for air purification performance of semiconducting photocatalytic materials – Part 1: Removal of nitric oxide, 2016.
[29] J.Z. Bloh, A. Folli, D.E. Macphee, Photocatalytic NO_x abatement: why the selectivity matters, RSC Adv. 4 (2014) 45726–45734, https://doi.org/10.1039/c4ra07916g.
[30] M.C. Lee, W. Choi, Solid phase photocatalytic reaction on the Soot/TiO_2 interface: the role of migrating OH, Radic., J. Phys. Chem. B. 106 (2002) 11818–11822, https://doi.org/10.1021/jp026617f.
[31] D. Kwon, S.H. Lee, J. Kim, T.H. Yoon, Dispersion, fractionation and characterization of sub-100nm P25 TiO_2 nanoparticles in aqueous media, Toxicol. Environ. Health Sci. 2 (2010) 78–85, https://doi.org/10.1007/BF03216516.
[32] M. Kosmulski, The pH dependent surface charging and points of zero charge. IX. Update, Adv. Colloid Interface Sci. 296 (2021), 102519, https://doi.org/10.1016/j.cis.2021.102519.
[33] M. Thommes, K. Kaneko, A.V. Neimark, J.P. Olivier, F. Rodriguez-Reinoso, J. Rouquerol, K.S.W. Sing, Physisorption of gases, with special reference to the evaluation of surface area and pore size distribution (IUPAC Technical Report, Pure Appl. Chem. 87 (2015) 1051–1069, https://doi.org/10.1515/pac-2014-1117.
[34] M. Kruk, M. Jaroniec, Gas adsorption characterization of ordered organic-inorganic nanocomposite materials, Chem. Mater. 13 (2001) 3169–3183, https://doi.org/10.1021/cm0101069.
[35] S. Link, M.A. El-Sayed, Size and temperature dependence of the plasmon absorption of colloidal gold nanoparticles, J. Phys. Chem. B 103 (1999) 4212–4217, https://doi.org/10.1021/jp984796o.
[36] Z. Lin, X. Wang, J. Liu, Z. Tian, L. Dai, B. He, C. Han, Y. Wu, Z. Zeng, Z. Hu, On the role of localized surface plasmon resonance in UV-Vis light irradiated Au/TiO_2 photocatalysis systems: pros and cons, Nanoscale 7 (2015) 4114–4123, https://doi.org/10.1039/c4nr06929c.
[37] K. Fujiwara, T. Akutsu, H. Gonome, Enhancing plasmon excitation of small Au nanoparticles via light scattering from metal-oxide supports, J. Phys. Chem. C. 126 (2022) 9509–9517, https://doi.org/10.1021/acs.jpcc.2c01566.
[38] M.M. Khan, S.A. Ansari, J. Lee, M.H. Cho, Enhanced optical, visible light catalytic and electrochemical properties of Au@TiO_2 nanocomposites, J. Ind. Eng. Chem. 19 (2013) 1845–1850, https://doi.org/10.1016/j.jiec.2013.02.030.
[39] N. Kruse, S. Chenakin, XPS characterization of Au/TiO_2 catalysts: binding energy assessment and irradiation effects, Appl. Catal. A Gen. 391 (2011) 367–376, https://doi.org/10.1016/j.apcata.2010.05.039.
[40] V. Jovic, W.-T. Chen, D. Sun-Waterhouse, M.G. Blackford, H. Idriss, G.I. N. Waterhouse, Effect of gold loading and TiO_2 support composition on the activity of Au/TiO_2 photocatalysts for H_2 production from ethanol–water mixtures, J. Catal. 305 (2013) 307–317, https://doi.org/10.1016/j.jcat.2013.05.031.
[41] J.F. Moulder, W.F. Stickle, W.M. Sobol, K. D., Handbook of X-Ray Photoelectron Spectroscopy, 1992.
[42] L. Wu, F. Li, Y. Xu, J.W. Zhang, D. Zhang, G. Li, H. Li, Plasmon-induced photoelectrocatalytic activity of Au nanoparticles enhanced TiO_2 nanotube arrays electrodes for environmental remediation, Appl. Catal. B Environ. 164 (2015) 217–224, https://doi.org/10.1016/j.apcatb.2014.09.029.
[43] J. Luo, J. Chen, H. Wang, H. Liu, Ligand-exchange assisted preparation of plasmonic Au/TiO_2 nanotube arrays photoanodes for visible-light-driven photoelectrochemical water splitting, J. Power Sources 303 (2016) 287–293, https://doi.org/10.1016/j.jpowsour.2015.11.016.
[44] R. Hernández, J.R. Hernández-Reséndiz, M. Cruz-Ramírez, R. Velázquez-Castillo, L. Escobar-Alarcón, L. Ortiz-Frade, K. Esquivel, Au-TiO_2 synthesized by a microwave- and sonochemistry-assisted sol-gel method: characterization and application as photocatalyst, Catalysts 10 (2020) 1052, https://doi.org/10.3390/catal10091052.
[45] D. Zhang, M. Wen, S. Zhang, P. Liu, W. Zhu, G. Li, H. Li, Au nanoparticles enhanced rutile TiO_2 nanorod bundles with high visible-light photocatalytic performance for NO oxidation, Appl. Catal. B Environ. 147 (2014) 610–616, https://doi.org/10.1016/j.apcatb.2013.09.042.
[46] S. Kashiwaya, J. Morasch, V. Streibel, T. Toupance, W. Jaegermann, A. Klein, The Work Function of TiO_2, Surfaces 1 (2018) 73–89, https://doi.org/10.3390/surfaces1010007.
[47] V. Mansfeldova, M. Zlamalova, H. Tarabkova, P. Janda, M. Vorokhta, L. Piliai, L. Kavan, Work function of TiO_2 (anatase, rutile, and brookite) single crystals: effects of the environment, J. Phys. Chem. C. 125 (2021) 1902–1912, https://doi.org/10.1021/acs.jpcc.0c10519.
[48] B. Gupta, A.A. Melvin, T. Matthews, S. Dash, A.K. Tyagi, TiO_2 modification by gold (Au) for photocatalytic hydrogen (H_2) production, Renew. Sustain. Energy Rev. 58 (2016) 1366–1375, https://doi.org/10.1016/j.rser.2015.12.236.
[49] I. Tanabe, T. Ryoki, Y. Ozaki, The effects of Au nanoparticle size (5–60 nm) and shape (sphere, rod, cube) over electronic states and photocatalytic activities of TiO_2 studied by far- and deep-ultraviolet spectroscopy, RSC Adv. 5 (2015) 13648–13652, https://doi.org/10.1039/c4ra12503g.
[50] M.C. Biesinger, L.W.M. Lau, A.R. Gerson, R.S.C. Smart, Resolving surface chemical states in XPS analysis of first row transition metals, oxides and hydroxides: Sc, Ti, V, Cu and Zn, Appl. Surf. Sci. 257 (2010) 887–898, https://doi.org/10.1016/j.apsusc.2010.07.086.
[51] A. Yoshida, Y. Mori, T. Ikeda, K. Azemoto, S. Naito, Enhancement of catalytic activity of Ir/TiO_2 by partially reduced titanium oxide in aerobic oxidation of alcohols, Catal. Today 203 (2013) 153–157, https://doi.org/10.1016/j.cattod.2012.04.020.
[52] Y. Yu, W. Wen, X.Y. Qian, J. Bin Liu, J.M. Wu, UV and visible light photocatalytic activity of Au/TiO_2 nanoforests with Anatase/Rutile phase junctions and controlled Au locations, Sci. Rep. 7 (2017) 1–13, https://doi.org/10.1038/srep41253.
[53] Y.F. Zhu, J. Zhang, L. Xu, Y. Guo, X.P. Wang, R.G. Du, C.J. Lin, Fabrication and photoelectrochemical properties of ZnS/Au/TiO_2 nanotube array films, Phys. Chem. Chem. Phys. 15 (2013) 4041–4048, https://doi.org/10.1039/c3cp43572e.
[54] T. Ohno, K. Sarukawa, K. Tokieda, M. Matsumura, Morphology of a TiO_2 photocatalyst (Degussa, P-25) consisting of anatase and rutile crystalline phases, J. Catal. 203 (2001) 82–86, https://doi.org/10.1006/jcat.2001.3316.
[55] M. Luna, J.M. Gatica, H. Vidal, M.J. Mosquera, One-pot synthesis of Au/N-TiO_2 photocatalysts for environmental applications: enhancement of dyes and NO_x photodegradation, Powder Technol. 355 (2019) 793–807, https://doi.org/10.1016/j.powtec.2019.07.102.
[56] X. Du, Y. Huang, X. Pan, B. Han, Y. Su, Q. Jiang, M. Li, H. Tang, G. Li, B. Qiao, Size-dependent strong metal-support interaction in TiO_2 supported Au nanocatalysts, Nat. Commun. 11 (2020) 1–8, https://doi.org/10.1038/s41467-020-19484-4.
[57] V.G. Bessergenev, M.C. Mateus, A.M. Botelho Do Rego, M. Hantusch, E. Burkel, An improvement of photocatalytic activity of TiO_2 Degussa P25 powder, Appl. Catal. A Gen. 500 (2015) 40–50, https://doi.org/10.1016/j.apcata.2015.05.002.
[58] V. Kumaravel, S. Mathew, J. Bartlett, S.C. Pillai, Photocatalytic hydrogen production using metal doped TiO_2: a review of recent advances, Appl. Catal. B Environ. 244 (2019) 1021–1064, https://doi.org/10.1016/j.apcatb.2018.11.080.
[59] J. Wang, P. Yang, B. Huang, Self-doped TiO_{2-x} nanowires with enhanced photocatalytic activity: facile synthesis and effects of the Ti^{3+}, Appl. Surf. Sci. 356 (2015) 391–398, https://doi.org/10.1016/j.apsusc.2015.08.029.
[60] S.Y. Lee, H.T. Do, J.H. Kim, Microplasma-assisted synthesis of TiO_2–Au hybrid nanoparticles and their photocatalytic mechanism for degradation of methylene blue dye under ultraviolet and visible light irradiation, Appl. Surf. Sci. 573 (2022), 151383, https://doi.org/10.1016/j.apsusc.2021.151383.
[61] L. Lin, X. Feng, D. Lan, Y. Chen, Q. Zhong, C. Liu, Y. Cheng, R. Qi, J. Ge, C. Yu, C. Duan, R. Huang, Coupling effect of Au nanoparticles with the oxygen vacancies

of TiO_{2-x} for enhanced charge transfer, J. Phys. Chem. C. 124 (2020) 23823–23831, https://doi.org/10.1021/acs.jpcc.0c09011.
[62] W. Zhu, S. Xiao, D. Zhang, P. Liu, H. Zhou, W. Dai, F. Liu, H. Li, Highly efficient and stable Au/CeO_2–TiO_2 photocatalyst for nitric oxide abatement: potential application in flue gas treatment, Langmuir 31 (2015) 10822–10830, https://doi.org/10.1021/acs.langmuir.5b02232.
[63] L. Lin, L. Yan, C. He, L. Yao, K. Xie, R. Chen, L. Zhu, J. Huang, J. Sun, J. Zhu, Z. Zhang, A theoretical study of the ability of 2D monolayer Au (111) to activate gas molecules, Int. J. Hydrog. Energy 46 (2021) 11711–11720, https://doi.org/10.1016/j.ijhydene.2021.01.060.
[64] A. Mills, J. Wang, M. Crow, Photocatalytic oxidation of soot by P25 TiO_2 films, Chemosphere 64 (2006) 1032–1035, https://doi.org/10.1016/j.chemosphere.2006.01.077.
[65] P. Chin, G.W. Roberts, D.F. Ollis, Kinetic modeling of photocatalyzed soot oxidation on titanium dioxide thin films, Ind. Eng. Chem. Res. 46 (2007) 7598–7604, https://doi.org/10.1021/ie070083t.
[66] B. Liu, J. Wang, J. Yang, X. Zhao, Charge carrier interfacial transfer pathways from TiO_2 and Au/TiO_2 nanorod arrays to electrolyte and the association with photocatalysis, Appl. Surf. Sci. 464 (2019) 367–375, https://doi.org/10.1016/j.apsusc.2018.09.031.
[67] L.-B. Xiong, J.-L. Li, B. Yang, Y. Yu, Ti^{3+} in the surface of titanium dioxide: generation, properties and photocatalytic application, J. Nanomater. 2012 (2012) 1–13, https://doi.org/10.1155/2012/831524.